Inorganic Chemistry

Article

pubs.acs.org/IC

Structural Frustration and Occupational Disorder: The Rare Earth Metal Polysulfides $Tb_8S_{14.8}$, $Dy_8S_{14.9}$, $Ho_8S_{14.9}$, and $Y_8S_{14.8}$

Thomas Doert,*[,†] Christian Graf,[†,⊥] Inga G. Vasilyeva,[‡] and Walter Schnelle[§]

[†]Department of Chemistry and Food Chemistry, Technische Universität Dresden, 01062 Dresden, Germany

[‡]Nikolaev Institute of Inorganic Chemistry, Siberian Branch of the Russian Academy of Sciences, 630090 Novosibirsk, Russia

[§]Max Planck Institute for Chemical Physics of Solids, 01187 Dresden, Germany

Supporting Information

ABSTRACT: Dark red crystals of $Y_8S_{14.8}$, $Tb_8S_{14.8}$, $Dy_8S_{14.9}$, and $Ho_8S_{14.9}$ have been obtained following different reaction routes. The isostructural title compounds adopt the Gd_8Se_{15} type, a 24-fold superstructure of the ZrSSi-type and can be described in space group $A112$ (non standard setting of $C121$, no. 5) with lattice parameter of a = 11.505(1) Å, b = 15.385(1) Å, c = 15.726(1) Å, and γ = 90.21(2)° for Y_8S_{15-x}; a = 11.660(1) Å, b = 15.468(2) Å, c = 15.844(2) Å, and γ = 90.19(2)° for Tb_8S_{15-x}; a = 11.584(1) Å, b = 15.340(2) Å, c = 15.789(2) Å, and γ = 90.34(2)° for Dy_8S_{15-x}; and a = 11.538(1) Å, b = 15.288(2) Å, c = 15.740(2) Å, and γ = 90.23(1)° for Ho_8S_{15-x}, respectively. The structure consists of an alternating stacking of puckered [*RES*] (*RE*, rare-earth metals) double slabs and planar sulfur layers along [001]. The planar sulfur layers have a complex arrangement of S_2^{2-} dinuclear dianions, isolated S^{2-} ions, and vacancies. All compounds contain trivalent rare-earth metal ions, for Tb_8S_{15-x} and Dy_8S_{15-x} antiferromagnetic order was found at T_N = 5.4(2) K and 3.8(1) K, respectively. Short wavelength cutoff optical band gaps of 1.6 to 1.7 eV were determined.

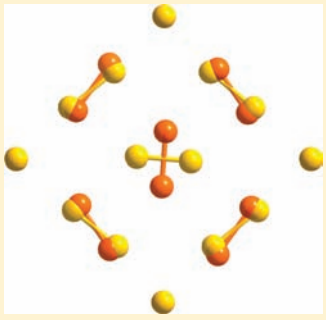

INTRODUCTION

The structural chemistry of the polychalcogenides of the trivalent rare-earth metals $REX_{2-\delta}$ (*RE* = Y, La–Nd, Sm, Gd–Lu, Lu; *X* = S, Se, Te; $0 \le \delta < 0.4$) is characterized by a multiplicity of compounds which exhibit closely related crystal structures with slightly different compositions.[1−4] The structures consist of an alternating stacking of puckered [*REX*] double layers and planar *X* layers and can be regarded as superstructures of the ZrSSi type.[5] Because of electronic reasons, covalent bonds are formed between the atoms of the planar chalcogen layers in the rare-earth polychalcogenides, which lead to structural distortions. As a result, the disulfides $RES_{2.0}$ and diselenides $RESe_{2.0}$ show a herringbone pattern of dumbbell-like S_2^{2-} and Se_2^{2-} dianions, respectively.[1] The chalcogen layers of the compounds $RES_{2-\delta}$ and $RESe_{2-\delta}$ with $\delta > 0$ exhibit defects and isolated X^{2-} anions besides dichalcogenide anions X_2^{2-}. The number of chalcogen defects and their assembly determine which kind of superstructure is realized.[2−4]

Three commensurate superstructures of the aristotype are known for rare-earth metal polysulfides and polyselenides: The $CeSe_2$ type, a 2-fold superstructure,[1] the $CeS_{1.9}$ type, a 10-fold superstructure with $\delta < 0.1$ (i.e. 10% chalcogen defects in the planar layers),[2] and the Gd_8Se_{15} type, a 24-fold superstructure ideally with δ = 0.125 (12.5% chalcogen defects in the planar layers).[3] Only for the latter structure type have additional chalcogen deficiencies been noticed. Compounds of the formula type $RESe_{2.0}$ and $RESe_{1.9}$ do not show such deviations. Chalcogen poorer polychalcogenides $REX_{2-\delta}$ with $\delta \ge 0.15$ tend to adopt incommensurately modulated variants of the aristotype.[4]

The structures of the rare-earth metal polysulfides $DyS_{1.77}$, $DyS_{1.836}$, and $HoS_{1.863}$ have been described in space group $P12_1/m1$ with lattice parameters of $a \approx c \approx 11$ Å, $b \approx 11.5$ Å, and $\beta \approx 91°$ in a model with an incomprehensible distribution of S^{2-} and S_2^{2-} anions in the planar layer.[6] There is, however, an alternative setting of the unit cell which allows for a more specific structural arrangement and which has been verified experimentally for a number of rare-earth metal polychalcogenides.[3] To have a concise description with the respective polyselenides RE_8Se_{15-x} (*RE* = Y, Gd, Tb, Dy, Ho, and Er) and to determine the compositions, we reinvestigated the polysulfides of the rare-earth metals Y, Dy, Tb, and Ho. The results are presented in the following sections.

EXPERIMENTAL SECTION

Syntheses. All preparation steps were carried out in an argon (99.996% Messer-Griesheim, Sulzbach, Germany) filled glovebox (MBraun, Garching, Germany). Crystals of the title compounds were obtained by flux reactions in KBr. For that 1 mmol of the rare-earth metals (Y, Tb, Dy, Ho; ingots 99.9% Strem Chemicals GmbH, Kehl, Germany) were rasped from compact blocks and filled in silica ampules with glassy carbon crucible together with 1.875 mmol of sulfur (99.9% powder, Fluka AG; Buchs, Switzerland; recrystallized in CS_2 and double sublimated) and 3 mmol of KBr (99.9% Merck GmbH, Darmstadt; molten under dynamic vacuum prior to use). The ampules were flame-sealed and placed in a furnace, heated to 1070 K for 10 days and cooled to room temperature with 3 K/h. The halide flux material was removed subsequently using a mixture of ethanol and water. Dark red crystals of

Received: July 31, 2011
Published: December 2, 2011

the polysulfides were obtained which are stable against atmospheric conditions and humidity. The use of KI as flux material at reaction temperatures of between 990 and 1070 K is also possible for the synthesis of crystals of these rare earth metal polysulfides.[7]

An alternative route is the preparation of Tb_8Se_{15-x} and Dy_8Se_{15-x} by metathesis according to the reaction scheme:

$$8RECl_3 + 12A_2S_2 \rightarrow RE_8S_{15} + 24ACl + 9S$$
$$(RE = \text{Tb–Ho};\ A = \text{Na, K})$$

This reaction type with an excess of chalcogen is known to produce the sulfur richest polysulfides in the binary systems accessible under ambient pressure conditions.[1f] It may, thus, also serve as a clear indication that polysulfides with a higher content of sulfur than the target compounds are not accessible under ambient pressure conditions. Anhydrous $RECl_3$ (powder, 99.9%) was used as obtained (Strem); K_2S_2 has been prepared by reaction of stoichiometric amounts of potassium (ingot, 99.99%, Chempur, Karlsruhe, Germany) with sulfur in liquid ammonia at 210 K; Na_2S_2 was obtained by reaction of sodium (99.9%, Fluka), H_2S (99.9%, Messer-Griesheim), and sulfur in ethanol (99%, Merck; dried with sodium and diethyl terephthalate prior use). The reaction mixtures were ground and filled in silica ampules with glassy carbon crucible inside. The ampules were flame-sealed, and the reaction mixtures were heated as described above. The excess sulfur formed during the reaction could be removed by sublimation. For that, the bottom of the ampule containing the reaction products was inserted in a vertical tubular furnace; the furnace temperature was held at 720 K for 20 h, for example; Sulfur deposits at the top of the ampule, which is kept outside the furnace. After opening the ampule, the alkali halide which intermediately acted as flux material for the crystallization of the polysulfide can be removed by rinsing the reaction product with a mixture of ethanol and water. Well-crystallized samples of Tb_8Se_{15-x} and Dy_8Se_{15-x} were obtained by this route, too. The reaction does not work out for Ho and Y polysulfides as ternary compounds are obtained, according to

$$2RECl_3 + 2Na_2S_2 \rightarrow NaRES_2 + Na_3RECl_6 + 2S$$
$$(RE = \text{Ho, Y})$$

According to X-ray data, the reaction paths stated above yield crystals of the same structure and composition within the experimental error. The structure data presented in the following is based on crystals from KBr flux reactions.[7b,8]

X-ray Powder Diffraction. X-ray powder diagrams (STOE Stadi-P powder diffractometer, Cu$K\alpha_1$ radiation, transmission setup) were recorded to check for phase purity. Lattice parameters were determined using the WINXPow software[9] and refined according to LeBail method[10] with the WinPlotR software.[11]

Single Crystal X-ray Diffraction. Buerger precession photographs were recorded for several crystals of each compound to check their quality and to predetermine the lattice parameters. Suitable crystals were subsequently placed on a diffractometer (STOE IPDS-II, Mo$K\alpha$ radiation, graphite monochromator), and complete data sets were recorded at 295 K. Integration of the data, as well as Lorentz and polarization factor corrections, have been performed with the IPDS software package.[12] A numerical absorption correction was applied based on the refined crystal shape using the programs XRED-97 and X-SHAPE.[13] The atomic positions of the respective selenides[3c] were taken as initial structure model for the refinements in JANA2006.[14] Extinction effects were corrected according to Becker and Coppens.[15]

Magnetic Properties. The temperature-dependent magnetization of samples of RE_8S_{15-x} was measured in a SQUID magnetometer (MPMS XL-7, Quantum Design) at external fields $\mu_0 H$ from 10 mT to 1 T in the temperature range 1.8 K–400 K. In addition, isothermal magnetization curves were taken at 1.8 K.

Chemical Analysis. The compositions of the flux grown samples were checked by EDX analyses (Noran Voyager system with a Si(Li) detector on a Zeiss DSM 982 Gemini microscope) and by atom spectroscopy (ICP-OES). For the latter 10 mg of the substances were sealed into 0.7 mm capillaries, which were cracked in an autoclave with PTFE inlay and digested using a 4 M HNO_3/HCl solution. The standard solutions as reference for the rare-earth metals and sulfur were taken from Johnson Matthey.

Experimental Densities. The densities of the flux grown crystals of RE_8S_{15-x} (RE = Tb–Ho) were determined with a Guy–Lussac type micropycnometer using between 1 and 10 crystals of about 0.005–0.01 g total mass and ethanol as a working liquid.[16] The density given in Table 1 is the average value of 10 measurements.

Table 1. Ratio S/*RE* for the Compounds RE_8S_{15-x} (RE = Y, Tb–Ho) Determined by Different Methods and Experimental Density ρ (g/cm^3)

RE metal	structure refinement	ICP-OES	tensimetry	ρ_{exp}[a]	structural formula (based on OES data)
Y	1.84(1)	1.85(2)			$YS_{1.85}$ ($Y_8S_{14.8}$)
Tb	1.83(1)	1.85(2)	1.85(2)	6.08(3)	$TbS_{1.85}$ ($Tb_8S_{14.8}$)
Dy	1.86(1)	1.86(2)	1.84(2)	6.28(5)	$DyS_{1.86}$ ($Dy_8S_{14.9}$)
Ho	1.85(1)	1.86(2)	1.86(2)	6.39(4)	$HoS_{1.86}$ ($Ho_8S_{14.9}$)

[a]For crystals grown from a KI flux.

Tensimetry. The static tensimetric-membrane-method permits to register the transitions from three-phase to the two-phase equilibria (and vice versa) by gradual changes in the composition of the original sample, owing to its incongruent vaporization in a closed system. The vapor pressures were measured using a Bourdon type manometer[17] upon heating. For these experiments, single crystals of the RE_8S_{15-x} compounds (RE = Tb, Dy, Ho) were loaded into the manometer and heated at 373 K under dynamic vacuum for 1 h. The manometer was sealed and then heated gradually. Pressure measurements are recorded after reaching the equilibrium at a given temperature. A scheme and the main characteristics of the experimental unit are described in detail in ref 18.

Optical Spectroscopy. Optical absorption spectra were recorded using a computerized diffraction MDR2 monochromator, combined with 25 or 400 W incandescent lamps and multipliers for measurements in a wide spectral range. For crystals of Tb_8S_{15-x}, Dy_8S_{15-x}, and Ho_8S_{15-x} of several millimeters thickness, the absorption spectra were obtained in polarized light at 300 K, and the short-wave edge of the transparency range was estimated from the extrapolation of the straight line approximating the $k^2(E)$ function to zero absorbance.

RESULTS AND DISCUSSION

X-ray Powder Data. X-ray powder diagrams of the RE_8S_{15-x} target compounds did not reveal any impurities (cf. Supporting Information).

Chemical Analysis and Experimental Density. Energy dispersive X-ray (EDX) analyses on clean crystal surfaces (obtained by cleaving or breaking immediately before the investigations) confirmed the absence of impurity elements and corroborated the composition within the accuracy of the method. The results of the inductively coupled plasma-optical emission spectrometry (ICP-OES) analyses on crystalline samples of the compounds RE_8S_{15-x} (RE = Y, Tb–Ho) are listed in Table 1, together with the refined compositions based on the X-ray data. In the two last columns the composition established from tensimetric studies and the experimental densities for crystals grown from a KI flux are given. The data show a good agreement of the compositions regardless of preparation route and experimental method.

Although the chemical composition may be expressed more easily with the formula $RES_{1.85(1)}$ we use the notation RE_8S_{15-x}

dx.doi.org/10.1021/ic201639f | Inorg. Chem. 2012, 51, 282–289

to emphasize the strong structural relationship to the selenides of the Gd_8Se_{15} type.[3c]

Magnetic Properties. For the calculation of the molar magnetic properties data a composition $RE_8S_{14.8}$ (x = 0.2) of the samples was adopted (cf. Table 1). As expected, Y_8S_{15-x} is diamagnetic (χ_0/Y-atom = $-37(20) \times 10^{-6}$ emu mol^{-1}) with a very small amount of Curie-paramagnetic impurities in the sample. The inverse magnetic susceptibilities $1/\chi(T) = H/M$ of Tb_8S_{15-x}, Dy_8S_{15-x} and Ho_8S_{15-x} follow the Curie–Weiss law only at high temperatures (see Figure 1). Deviations at lower temperature are due to the large splitting of the respective Hund's rule ground multiplets by crystal fields. The effective paramagnetic moments μ_{eff} and the paramagnetic Weiss temperatures Θ_P from fits to the data above 100 K are given in Table 2. The observed values of μ_{eff} are in fair agreement with the free-ion values of the respective trivalent rare-earth ions.[19] The Θ_P values are strongly influenced by the crystal field splitting. It is however possible that the quite large positive Θ_P values for Tb_8S_{15-x} and especially for Ho_8S_{15-x} indicate some ferromagnetic nearest-neighbor interaction.

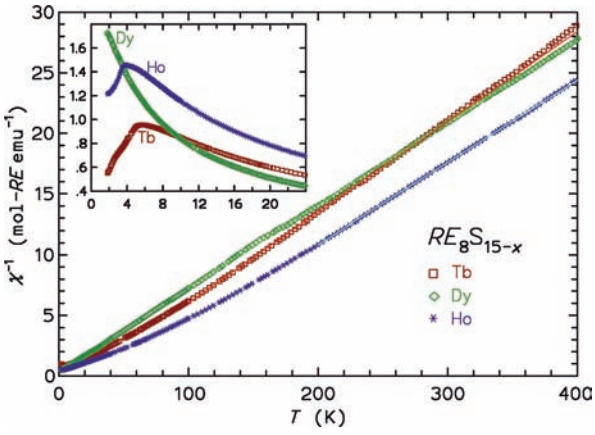

Figure 1. Inverse magnetic susceptibilities $1/\chi(T)$ per *RE*-atom vs temperature for samples of RE_8S_{15-x} (*RE* = Tb, Dy, Ho) for a field μ_0H = 1.0 T. The lines (almost coinciding with the data markers) are Curie–Weiss fits to the data. The inset shows the magnetic susceptibility $\chi(T)$ in emu (mol-*RE*)$^{-1}$ for low temperatures in a field μ_0H = 10 mT.

At low temperatures, typical cusps in $\chi(T)$ because of long-range antiferromagnetic ordering of the rare-earth moments are observed for the Tb and Ho compound (Figure 1 inset; Tb_8S_{15-x}: Néel temperature T_N = 5.4(2) K; Ho_8S_{15-x}: T_N = 3.8(2) K). No ferromagnetic ordering components were observed. A magnetic ordering in Dy_8S_{15-x} could not be detected for temperatures above 1.9 K.

The isothermal magnetization at 1.8 K (Supporting Information, Figure 2) increases steeply up a field of about 3 T and then keeps on increasing with smaller slope up to our highest measured field of 7 T. At this field the specific magnetizations of 7.4, 6.1, and 8.8 μ_B/*RE*-atom are attained, which are well below the expected saturation values of $\mu_{sat} = gJ$ of 9, 10, and 10 μ_B/*RE*-atom, for Tb_8S_{15-x}, Dy_8S_{1-x}, and Ho_8S_{15-x}, respectively. The polycrystalline nature of the sample and the broad ordering transitions (probably owing to the disordered structure) allow no further speculation on the magnetic ordering.

Crystal Structure. The dimensions of the *A*-centered unit cells of the investigated rare-earth metal polysulfides are found in the ranges 11.505(1) Å ≤ a ≤ 11.660(1) Å, 15.288(2) Å ≤ b ≤ 15.468(2) 15.5 Å, 15.740(2) Å ≤ c ≤ 15.789(2) Å, and 90.19(2)° ≤ γ ≤ 90.34(2)° and are very similar to those of the respective polyselenides of the Gd_8Se_{15} type (orthorhombic space group *Amm*2, no. 38).[3c] However, in contrast to the polyselenides, one angle was found to deviate from 90° (cf. Table 3) and structure refinements in *Amm*2 yielded unreasonable high residuals and difference electron density peaks, so that a symmetry reduction to the monoclinic subgroup *A*112 (nonstandard setting of *C*121, no. 5) was deemed prudent. To have the atomic positions as close as possible to the ones of the polyselenides RE_8S_{15-x} (*RE* = Y, Gd–Er) and to extend the group-subgroup relations established with the Bärnighausen tree by Stöwe[3b] we chose the nonstandard setting of *A*112 for the structure refinement with the origin in z fixed in S19. With this choice planar sulfide layers are found at $z \approx 0$ and $z \approx 1/2$. The atom labeling scheme was also developed following the Bärnighausen scheme (Supporting Information; only the positions in the planar sulfide layer are given). From a crystal-chemical point of view, the chalcogen vacancies can be treated as normal Wyckoff sites as has been discussed for the compounds of the $CeS_{1.9}$ and the Gd_8Se_{15} type.[2f,3b,c] The symmetry reduction from *Amm*2 to *A*112 does not change the multiplicity of the vacant sites, and we can expect a 2-fold and a 4-fold vacant site, vide infra.

All crystals were found to be multiple twinned, as can be expected from several *translationengleiche* symmetry reduction steps in the Bärnighausen tree. The investigated crystals of Y_8S_{15-x}, Tb_8S_{15-x}, Dy_8S_{15-x}, and Ho_8S_{15-x} were finally refined as 4-fold twins as given in Table 3.

In addition to the high pseudosymmetry and twinning of the structures, disorder on several sulfur sites impede a straightforward structure solution. These items lead, for example, to strong correlations in the refinements, which were minimized by considering only isotropic displacement for the sulfur atoms in the final refinement runs. Moreover, for Dy_8S_{15-x} 12 reflections with intensities above the detection threshold of $I > 3\sigma(I)$ were found to violate the *A* centering which points toward space group *P*112 (no. 3). In the primitive cell, however, even larger correlations occur, and a stable refinement is impossible so that the final structure model was developed in *A*112, too.

The results of the structure determination and relevant crystallographic data are listed in Tables 3 and selected interatomic distances in Table 4. Note the good agreement of the theoretical

Table 2. Magnetic Data for the Compounds RE_8S_{15-x} (*RE* = Y, Tb, Dy, Ho): Effective Paramagnetic Moment (Observed, Free-Ion Value[19]), Weiss Temperature, and Magnetic Long-Range Ordering Type and Temperatures

	μ_{eff} (obs.) (μ_B/*RE*-atom)	μ_{eff} (free-ion) (μ_B/*RE*-atom)	Θ_P (K)	magnetic order/phase transitions	T_N (K)
Y_8S_{15-x}	0.06	0	n. a.	none	
Tb_8S_{15-x}	10.4	9.72	+18.6	antiferromagnetic	5.4(2)
Dy_8S_{15-x}	10.9	10.65	−7.7	none (T > 1.9 K)	
Ho_8S_{15-x}	10.9	10.61	+40.4	antiferromagnetic	3.8(1)

dx.doi.org/10.1021/ic201639f | *Inorg. Chem.* 2012, 51, 282–289

Table 3. Crystallographic Data for Y_8S_{15-x}, Tb_8S_{15-x}, Dy_8S_{15-x}, and Ho_8S_{15-x} at T = 295(2) K

sum formula	$YS_{1.85}$	$TbS_{1.85}$	$DyS_{1.86}$	$HoS_{1.86}$
deposition number[a]	CSD-422950	CSD-422951	CSD-422952	CSD-422953
diffractometer, radiation	Stoe IPDS−II, Mo$K\alpha$			
crystal system, space group, Z	monoclinic, $A112$, 48			
lattice parameters				
a (Å)	11.505(1)	11.660(1)	11.584(1)	11.538(1)
b (Å)	15.385(2)	15.468(2)	15.340(2)	15.288(2)
c (Å)	15.726(2)	15.844(2)	15.789(2)	15.740(2)
γ (deg)	90.21(2)	90.19(2)	90.34(2)	90.23(2)
cell volume V (Å^3)	2783.9(6)	2857.6(6)	2805.6(6)	2776.4(6)
calculated density ρ (g·cm^{-3})	4.23	6.06	6.31	6.43
abs. coefficient μ (mm^{-1})	26.4	30.9	33.2	35.4
F(000)	3284	4520	4592	4635
crystal size (mm^3)	0.02 × 0.04 × 0.05	0.02 × 0.07 × 0.10	0.02 × 0.04 × 0.05	0.01 × 0.04 × 0.06
abs. correction	numerical[13]			
T_{min}, T_{max}	0.198, 0.305	0.084, 0.230	0.136, 0.317	0.097/0.279
measuring range0	$2.56° \le \theta \le 32.11°$	$2.55° \le \theta \le 31.90°$	$2.55° \le \theta \le 31.88°$	$2.56° \le \theta \le 33.48°$
hkl−range	$-17 \le h \le 16$; $-22 \le k \le 22$; $-23 \le l \le 23$	$-17 \le h \le 17$; $-22 \le k \le 22$; $-22 \le l \le 23$	$-17 \le h \le 17$; $-22 \le k \le 22$; $-20 \le l \le 23$	$-16 \le h \le 17$; $-23 \le k \le 23$; $-24 \le l \le 24$
reflections collected/independent	33754/9566	33923/9378	42579/8909	34033/10781
R_{int}, R_σ	0.073, 0.023	0.063, 0.015	0.088, 0.027	0.074, 0.035
refinement method	JANA2006;[14] full matrix against F^2			
constraints/parameter	16/232	16/232	16/232	16/232
goodness of fit	2.10	1.35	1.12	1.22
R_1, wR_2 [$I > 3\sigma(I)$]	0.056, 0.110	0.039, 0.097	0.026, 0.054	0.036, 0.068
R_1, wR_2 (all I)	0.083, 0.116	0.048, 0.100	0.044, 0.061	0.066, 0.073
extinction parameter	0.352(1)	0.042(2)	0.544(5)	0.050(1)
electron density (e·Å^{-3})	2.06/−1.53	2.03/−2.04	2.84/−1.54	1.70/−1.87
twin matrices	(−1 0 0, 0 −1 0, 0 0 −1); (1 0 0, 0 −1 0, 0 0 −1); (−1 0 0, 0 1 0, 0 0 1)			
twin volume fractions (%)	20(3), 37(2), 14(2), 29(2)	0.35(4), 16(2), 14(2), 36 (2)	25(4), 25(2), 25(2), 25(2)	19(5), 31(3), 23(3), 28(3)

[a]Structure data have also been deposited at FIZ Karlsruhe, 76344 Eggenstein-Leopoldshafen, Germany, and can be obtained free of charge on quoting the deposition numbers (http://www.fiz-karlsruhe.de/request_for_deposited_data.html).

Table 4. Selected Interatomic Distances (Å) for $TbS_{1.875-x}$, $DyS_{1.875-x}$, $HoS_{1.875-x}$, and $YS_{1.875-x}$

	Tb_8S_{15-x}	Dy_8S_{15-x}	Ho_8S_{15-x}	Y_8S_{15-x}
[RE−S][a]	2.735(9)−3.00(1)	2.725(9)−2.951(9)	2.700(7)−2.95(1)	2.707(7)−2.953(7)
[RE]−[S][b]	2.70(1)−3.29(2)	2.68(4)−3.24(4)	2.65(5)−3.23(4)	2.66(2)−3.23(2)
S(15a)−S(24b)	2.13(2)	2.20(2)	2.25(3)	2.27(2)
S(15b)−S(24a)	2.27(2)	2.05(3)	2.18(2)	2.18(2)
S(16a)−S(23b)	2.26(2)	2.18(2)	2.28(2)	2.16(2)
S(16b)−S(23a)	2.07(1)	2.14(3)	2.12(3)	2.06(1)
S(17a)−S(20a)	2.18(2)	2.16(2)	2.20(3)	2.27(2)
S(17b)−S(21b)	2.12(2)	2.10(2)	2.16(2)	2.18(2)
S(18a)−S(21a)	2.34(2)	2.40(5)	2.29(5)	2.11(1)
S(18b)−S(20b)	2.19(3)	2.36(5)	2.40(7)	2.11(2)
S(22a)−S(22a)	2.543(1)	2.131(8)	2.17(2)	2.34(1)
S(22b)−S(22b)	2.240(8)	2.15(1)	2.14(1)	2.143(7)

[a]RE−S distances in the puckered double slabs. [b]RE−S distances between RE atoms and S atoms of the planar layers.

density with the experimental data in Table 1. Further crystallographic information can be found in the Supporting Information.

Like the respective polyselenides RE_8Se_{15-x} (RE = Y, Gd−Er), the title compounds Y_8S_{15-x}, Tb_8S_{15-x}, Dy_8S_{15-x}, and Ho_8S_{15-x} represent 24-fold superstructures of the ZrSSi type with cell parameters $a \approx 3a_0$, $b \approx 4a_0$, and $c \approx 2c_0$ but with obvious monoclinic cell metrics. As the four title compounds are isotypic the description and discussion of their structures will be given on the example Y_8S_{15-x} in detail.

As stated above, the structure of Y_8S_{15-x} consists of an alternative stacking of puckered double slabs of yttrium (Y1−Y13) and sulfur (S1−S13) and planar sulfur layers (S14−S24) along [001] Figure 2. Especially from the left part of Figure 2, the similarity to the aristotype is apparent. The distances from Y to the S atoms of the puckered double slabs as well as to those in the planar layers range from 2.66 Å to 3.23 Å and are typical for rare-earth metal poly(sulfides).[1−4]

The main differences compared to the ZrSSi type can be found in the planar chalcogen layers which are chalcogen deficient.

dx.doi.org/10.1021/ic201639f | Inorg. Chem. 2012, 51, 282−289

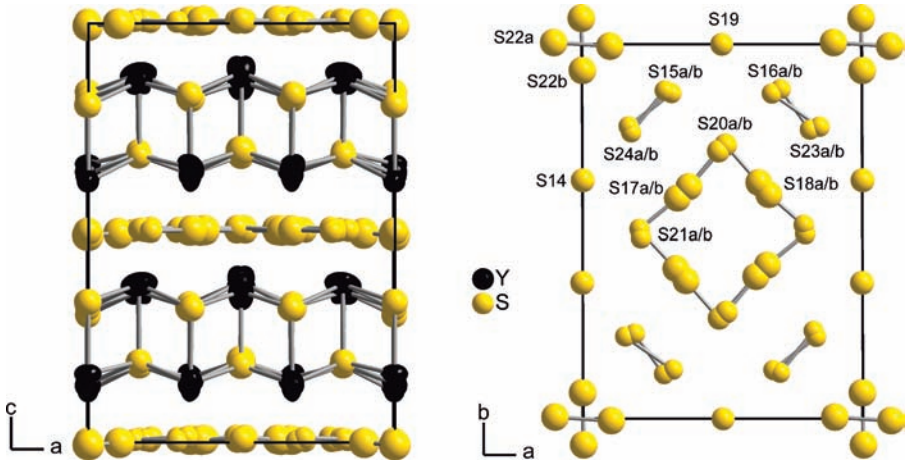

Figure 2. Unit cell of Y_8S_{15-x} (left) and split positions of the planar sulfur layer (right, $z \approx 0$), atoms at a 99.9% probability level.

Because of the vacancies and under consideration of the disorder in the sulfur layer, the coordination number (CN) for some of the metal atoms is reduced from 9 for a fully occupied planar layer to 7 (Y3) or 8 (Y1, Y7, Y8, Y12, and Y13), respectively, if a threshold of 3.15 Å for the first coordination sphere is chosen. Y2, Y4, Y5, Y6, Y 9, Y10, and Y11, retain a 9-fold coordination. The coordination polyhedra can be described as distorted capped (CN 7), bicapped (CN 8), and tricapped (CN 9) trigonal prisms, Figure 3.

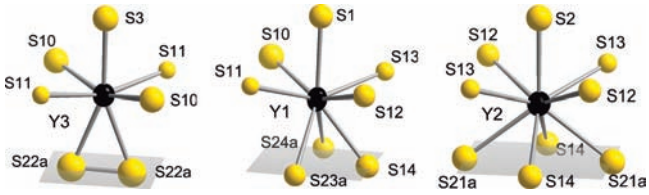

Figure 3. Examples for coordination number 7 (Y3, left), CN 8 (Y1, center), and CN 9 (Y2, right); only one split position for the S atoms of the planar sulfur layer (right, $z \approx 0$), atoms at a 99.9% probability level, planar sulfide layer indicated by a gray plane.

The planar sulfur layer of Y_8S_{15-x} looks somewhat confusing at a first glance, right part of Figure 2. One central feature is the vacancy at (1/2, 1/2, 0) which is surrounded by a ring-like arrangement of sulfur atoms. As can be expected from the structural image, a simultaneous occupancy of all S positions is not possible as interatomic distances that are too short would result. The refinement of the respective sulfur sites as partially occupied split positions shows that the vacancy is indeed surrounded by eight sulfur atoms forming a homodromic arrangement of four S_2^{2-} dianions in two different orientations, Figure 4 (left and center). We will refer to this entity as "eight-membered ring" in the following discussion. An analogous superposition of such entities has also been discussed for the rare-earth metal polyselenides RE_8Se_{15-x} (RE = Y, Gd–Er).[3c] Sulfur (split) positions S18a/b, S17a/b, S20a/b, and S21a/b are involved in the disordered eight-membered ring of Y_8S_{15-x}. The distances within the S_2^{2-} dianions are found between 2.11 Å and 2.29 Å. With respect to the disorder, these distances are in reasonable agreement with distances of other or rare-earth metal polysulfides.[1d,f,2d–f] The distances between the dianions in the eight-membered ring are found in the range from 2.50 Å to 2.70 Å. These distances between different anions are significantly shorter than the van der Waals distance of sulfur (3.6 Å)[20] even if the disorder is taken into account. Partially bonding interactions must hence be considered for these dianions. Distances significantly shorter than the van der Waals distance have been found between the Se_2^{2-} dianions in the polyselenides RE_8Se_{15-x} (RE = Y, Gd–Er) were the integrated crystal orbital Hamiltonian population (ICOHP)[21] was computed to values up to −0.93 eV (for a distances of 2.78 Å) between two Se_2^{2-} dianions.[3c]

The remaining atoms of the planar layer of Y_8Se_{15-x} are grouped into disordered S_2^{2-} dianions ($(S15a–S24b)^{2-}$/$(S15b–S24a)^{2-}$, $(S16a–S23b)^{2-}$/$(S16b–S23a)^{2-}$, and $(S22a–S22a)^{2-}$/$(S22b–S22b)^{2-}$) and isolated S^{2-} anions (S14 and S19).

As discussed above, in the nondisordered 24-fold superstructure of Y_8Se_{15-x}, two vacancies with different multiplicities should occur, one at Wyckoff site 4*c* and one at Wyckoff site 2*b* (cf. Bärnighausen tree in the Supporting Information). For charge compensation, each vacancy should be accompanied by a S^{2-} anion. The single S^{2-} anions S14 (Wyckoff site 4*c*) and

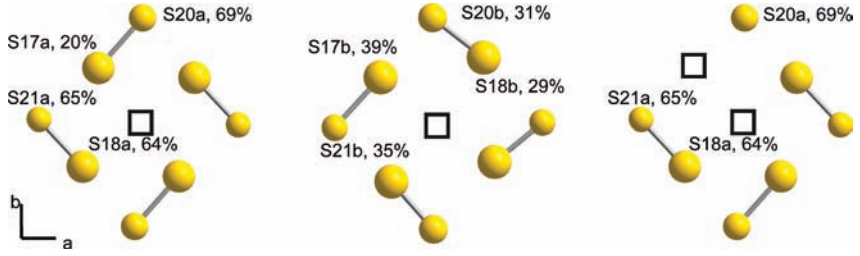

Figure 4. Possible orientations of the S_2^{2-} dianions around the vacancy (left and center), and scenario with two adjacent vacancies (right); atoms at a 99.9% probability level.

dx.doi.org/10.1021/ic201639f | *Inorg. Chem.* 2012, 51, 282–289

S19 (Wyckoff site 2*b*) and the vacancy at (1/2, 1/2, 0), Wyckoff site 2*b*, can easily be seen in the image of the planar layer, Figure 2. The second vacancy on Wyckoff site 4*c*, although surely existent, is not visible in that image because of positional disorder of the disulfide anion $(S22a–S22a)^{2-}$/$(S22b–S22b)^{2-}$. If position S22a, and hence dianion $(S22a–S22a)^{2-}$, is present the position of S22b is vacant and vice versa (cf. Figure 5).

Following with this idealized structure model, 21 sulfur positions out of 24 possible ones are occupied per planar layer. The 21 sulfur atoms are grouped into nine S_2^{2-} dianions and three S^{2-} anions resulting in the formula $[(S^{2-})_3(S_2^{2-})_9\square_3]$ for the layer ($\square$ denotes a vacancy). This idealized pictures would yield a composition Y_8S_{15} or $YS_{1.875}$.

However, the situation is somewhat more complicated because of further occupational peculiarities which can best be seen from Fourier maps (F_o) of the sulfur layer, Figure 6. The areas around atoms S17a/b and S18a/b are characterized by lower electron densities compared to those of other S positions. An unrestrained refinement of the occupancies of these split positions yielded 0.28(2) for S17a and 0.39(2) for S17b and 0.63(2) for S18a and 0.26(2) for S18b leading to the formula $Y_8Se_{14.7}$ or $YSe_{1.84}$, which is in good agreement with the results of the chemical analysis. The impact of the additional sulfur deficiency for the eight-membered ring is visualized in the right part of Figure 4. If, for example, S17 is missing a further S^{2-} anion (S20a in this case) must be generated for charge compensation. The motif of two adjacent vacancies in this scenario is known from the incommensurately modulated structures of $RESe_{1.84(1)}$, (*RE* = La–Nd, Sm).[4]

The disorder of the eight-membered ring can be understood as a consequence of structural frustration. In defective layers containing X_2^{2-} anions as well as X^{2-} anions (*X* = S, Se), the X^{2-} anions tend to have a radial surrounding by four X_2^{2-} dianions for energetic reasons. This has been shown theoretically for rare-earth metal polyselenides[22] and was found true experimentally for all rare-earth polysulfides and polyselenides adopting the $CeSe_{1.9}$ structure type.[2] The $CeSe_{1.9}$ type is the only structure type known up to now with a fully ordered radial surrounding of all X^{2-} anions. In the planar layers of the more defective title compound Y_8S_{15-x}, only S19 has this radial environment with $(S15a–S24b)^{2-}$/$(S15b–S24a)^{2-}$ (2×) and $(S16a–S23b)^{2-}$/$(S16b–S23a)^{2-}$ (2×). S14 has anions $(S15a–S24b)^{2-}$/$(S15b–S24a)^{2-}$ and $(S16a–S23b)^{2-}$/$(S16b–S23a)^{2-}$ as neighbors on the one side, but can either have $(S21a–S18a)^{2-}$ or $(S21b–S17b)^{2-}$ on the other as the latter two dinuclear anions belong to two different orientations of the homodromic eight-membered ring, Figure 4.

The disorder of the anions $(S22a–S22a)^{2-}$/$(S22b–S22b)^{2-}$ on the other hand may cause the disorder of the anions $(S15a–S24b)^{2-}$/$(S15b–S24a)^{2-}$ and $(S16a–S23b)^{2-}$/$(S16b–S23a)^{2-}$. As shown in Figure 5, the rectangular arrangement of 12 S atoms around the central $(S22–S22)^{2-}$ anion seems to relax: By changing from position S22a to S22b, the anions $(S15–S24)^{2-}$ and $(S16–S23)^{2-}$ seem to tilt around their centers of gravity to avoid short distances between the central dinuclear anion and the surrounding ones. The structure type is obviously able to adjust for different disordered arrangements within certain limits.

Another possible feature should be mentioned here. The RE_8S_{15-x} crystals may be intergrown on the atomic scale, meaning that small domains of slightly different ordering and/or

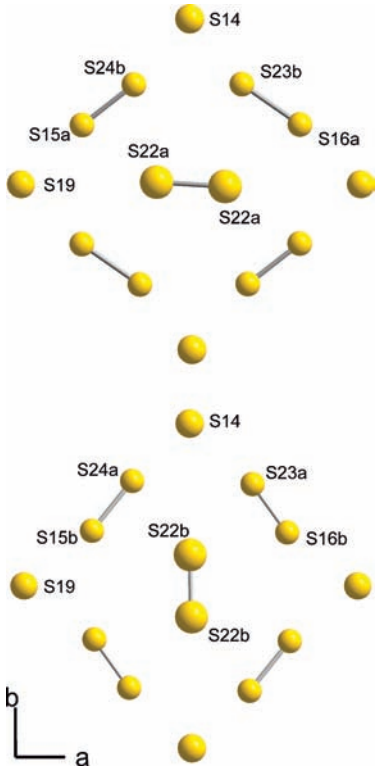

Figure 5. Dianions $(S22a–S22a)^{2-}$ and $(S22b–S22b)^{2-}$ and their environments; atoms at a 99.9% probability level.

compositions may exist. Their X-ray scattering contributions may then superimpose coherently and incoherently depending on the domain size. A resolution hereof is beyond the current state of the art of the method. Moreover, the quality of the RE_8S_{15-x} crystals, based on their scattering images, is subject to changes depending on the crystallization condition. In crystals of some reaction batches, the disorder manifests itself in noticeable streaking of reflections

Structures of RE_8S_{15-x} (RE = Tb, Dy, and Ho). At a first glance the structures of the three compounds Tb_8S_{15-x}, Dy_8S_{15-x}, and Ho_8S_{15-x} seem not to differ from that of Y_8S_{15-x} discussed above (structure images with sections of the structures are given in the Supporting Information). However, small but significant differences occur in the planar sulfide layers, which can best be visualized from the respective Fourier maps (F_o), Figure 6. The electron densities in the region of S17, S18, and S21 alter from compound to compound resulting in slightly different compositions. Moreover, the electron density in the area of S22a and S22b differs markedly. As a result the position of S22a in Dy_8S_{15-x} is occupied predominantly with an occupancy of approximately 60%. In Tb_8S_{15-x}, Ho_8S_{15-x}, and Y_8S_{15-x} however, the occupation of S22b is favored (58%, 61%, and 60%, respectively). For the respective selenides RE_8Se_{15-x} (*RE* = Y, Gd–Er) an increasing occupancy probability for the dianion parallel [010] (S22b) with decreasing rare-earth metal size was observed.[3c] It is, however, not yet understood why the occupancies of S22a/b in Dy_8S_{15-x} do not fit into this series.

Optical Spectroscopy. The optical absorption edges determined at *T* = 300 K are 770 nm (1.6 eV) for Tb_8S_{15-x}, 769 nm (1.6 eV) for Dy_8S_{15-x} and 722 nm (1.7 eV) for Ho_8S_{15-x}. Crystals of the title compounds, as those of the

dx.doi.org/10.1021/ic201639f | *Inorg. Chem.* 2012, 51, 282–289

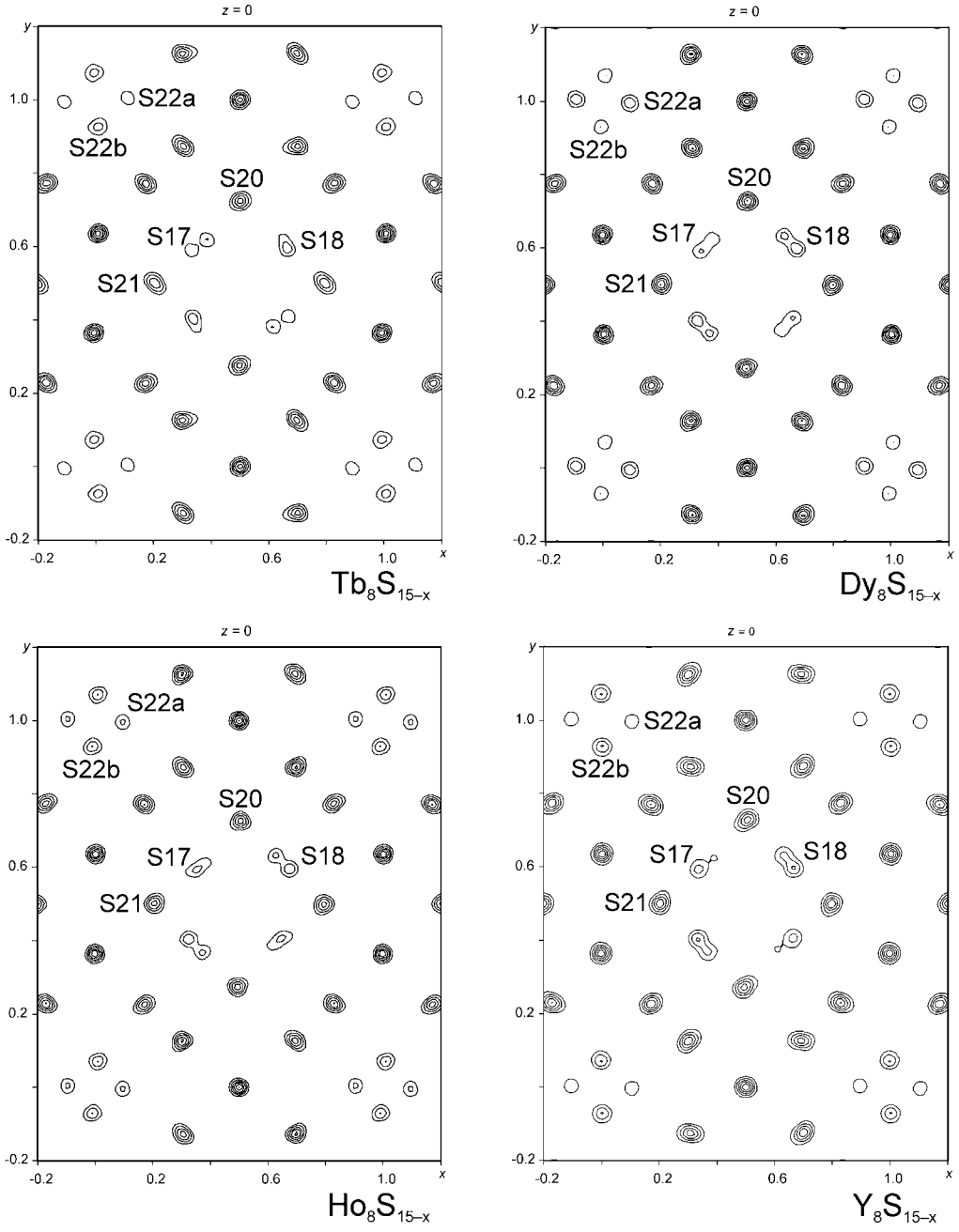

Figure 6. Fourier maps (F_o) for Tb_8S_{15-x} (top left), Dy_8S_{15-x}, (top right), Ho_8S_{15-x}, (bottom left), and Y_8S_{15-x}(bottom right) at $z \approx 0$ (electron densities have been summed up between $-0.04 \leq z \leq 0.04$, contour lines correspond to a difference of 5 e·Å^3).

majority of rare earth metal polysulfides and polyselenides, appear lustrous red or dark red.

SUMMARY

Deep red crystals of $Tb_8S_{14.8}$, $Dy_8S_{14.9}$, $Ho_8S_{14.9}$, and $Y_8S_{14.8}$ have been prepared by different reaction routes, and their structures have been reinvestigated. The compounds adopt a 24-fold superstructure of the ZrSSi-type which can be attributed to be of the Gd_8Se_{15} type but with lowered symmetry (space group *A*112, no. 5). The structures consist of puckered [*RES*] double slabs and planar sulfur layers which exhibit a strongly disordered arrangement of S_2^{2-} dianions, isolated S^{2-} anions and vacancies. The compounds contain trivalent rare-earth metal ions and have band gaps of about 1.6−1.7 eV. Tb_8S_{15-x} and Ho_8S_{15-x} show antiferromagnetic ordering at T_N = 5.4(2) K and T_N = 3.8(2) K), respectively.

ASSOCIATED CONTENT

Supporting Information

The PDF file contains examples for experimental and theoretical X-ray powder diagrams (incl. a LeBail fit for Ho_8Se_{15-x}), the structure images of Tb_8S_{15-x}, Dy_8S_{15-x}, and Ho_8S_{15-x}, the Bärnighausen scheme for the atomic positions of the planar chalcogen layers derived from the ZrSSi type; for Gd_8Se_{15}[3c] and Y_8S_{15-x} and the isothermal magnetization curves for Tb_8S_{15-x}, Dy_8S_{15-x}, and Ho_8S_{15-x} at 1.8 K. The CIF file contains the crystallographic information files (cif-format) of the compounds Y_8S_{15-x}, Tb_8S_{15-x}, Dy_8S_{15-x}, and Ho_8S_{15-x}. This material is available free of charge via the Internet at http://pubs.acs.org.

dx.doi.org/10.1021/ic201639f | *Inorg. Chem.* 2012, 51, 282−289

AUTHOR INFORMATION

Corresponding Author

*E-mail: thomas.doert@chemie.tu-dresden.de. Phone: +49-351-463-33864. Fax: +49-351-463-37287.

Present Address

[⊥]Chemische Fabrik Budenheim, D-55257 Budenheim, Germany.

ACKNOWLEDGMENTS

The authors thank Dr. G. Auffermann (MPI-CPfS, Dresden) for chemical analyses, E. Kern (TU Dresden) for the EDX analyses. Financial support of the Deutsche Forschungsgemeinschaft is gratefully acknowledged.

REFERENCES

(1) (a) Marcon, J. P.; Pascard, R. *C. R. Acad. Sci., Ser. C* **1968**, *266*, 270. (b) Bénazeth, S.; Carré, D.; Laruelle, P. *Acta Crystallogr.* **1982**, *B38*, 33. (c) Bénazeth, S.; Carré, D.; Laruelle, P. *Acta Crystallogr.* **1982**, *B38*, 37. (d) Tamazyan, R.; Arnold, H.; Molchanov, V. N.; Kuzmicheva, G. M.; Vasilyeva, I. G. *Z. Kristallogr.* **2000**, *215*, 272. (e) Doert, Th.; Graf, C. *Z. Allg. Anorg. Chem.* **2005**, *631*, 1101. (f) Schleid, T.; Lauxmann, P.; Graf, Ch.; Bartsch, Ch.; Doert, Th. *Z. Naturforsch.* **2009**, *64b*, 189. (g) Müller, C. J.; Schwarz, U.; Schmidt, P.; Schnelle, W.; Doert, Th. *Z. Allg. Anorg. Chem.* **2010**, *636*, 947. (h) Müller, C. J.; Doert, Th.; Schwarz, U. *Z. Kristallogr.* **2011**, *226*, 646.

(2) (a) Plambeck-Fischer, P.; Abriel, W.; Urland, W. *J. Solid State Chem.* **1989**, *78*, 164. (b) Urland, W.; Plambeck-Fischer, P.; Grupe, M. *Z. Naturforsch.* **1989**, *44b*, 261. (c) Grupe, M.; Urland, W. *J. Less-Common Met.* **1991**, *170*, 271. (d) Tamazyan, R.; Arnold, H.; Molchanov, V. N.; Kuzmicheva, G. M.; Vasilyeva, I. G. *Z. Kristallogr.* **2000**, *215*, 346. (e) Dashjav, E.; Doert, Th.; Böttcher, P.; Mattausch, Hj.; Oeckler, O. *Z. Kristallogr. NCS* **2000**, *215*, 337. (f) Doert, Th.; Graf, Ch.; Lauxmann, P.; Schleid, Th. *Z. Anorg. Allg. Chem.* **2007**, *633*, 2719.

(3) (a) Adams, K. G. Diploma Thesis, University of Karlsruhe, Karlsruhe, Germany, 1993. (b) Stöwe, K. *Z. Kristallogr.* **2001**, *216*, 215. (c) Doert, Th.; Dashjav, E.; Fokwa, B. P. T. *Z. Anorg. Allg. Chem.* **2007**, *633*, 261.

(4) (a) van der Lee, A.; Hoistad, L. M.; Evain, M.; Foran, B. J.; Lee, S. *Chem. Mater.* **1997**, *9*, 218. (b) Tamazyan, R.; van Smaalen, S.; Vasilyeva, I. G.; Arnold, H. *Acta Crystallogr.* **2003**, *B59*, 709. (c) Doert, Th.; Graf, C.; Schmidt, P.; Vasilyeva, I. G.; Simon, P.; Carrrillo-Cabreras, W. *J. Solid State Chem.* **2007**, *180*, 501. (d) Graf, C.; Doert, Th. *Z. Kristallogr.* **2009**, *224*, 568.

(5) Onken, H.; Vierheilig, K.; Hahn, H. *Z. Anorg. Allg. Chem.* **1964**, *333*, 267.

(6) (a) Tamazyan, R. A.; Molchanov, V. N.; Kuzmicheva, G. M.; Vasilyeva, I. G. *Russ. J. Inorg. Chem.* **1994**, *39*, 397. (b) Podberezskaya, N. V.; Naumov, D. Yu.; Vasilyeva, I. G.; Pervukhina, N. V.; Magarill, S. A.; Borisov, S. V. *J. Struct. Chem.* **1998**, *39*, 710. (c) Podberezskaya, N. V.; Pervukhina, N. V.; Belaya, S. V.; Vasilyeva, I. G.; Borisov, S. V. *J. Struct. Chem.* **2001**, *42*, 617. (d) Belaya, S. V.; Vasilyeva, I. G.; Pervukhina, N. V.; Podberezskaya, N. V.; Eliseev, A. P. *J. Alloys Compd.* **2001**, *323*−*324*, 26.

(7) (a) Vasilyeva, I. G. *Russ. J. Phys. Chem.* **2006**, *80*, 1842. (b) Graf, C. Ph.D. Thesis, Technische Universität Dresden, Dresden Germany, 2008.

(8) Schleid, Th.; Lissner, F. *Eur. J. Solid State Inorg. Chem.* **1993**, *30*, 829.

(9) *WinXPOW, powder diffraction software*; STOE & Cie.: Darmstadt, Germany, 2003.

(10) LeBail, A.; Duroy, H.; Fourquet, J. L. *Mater. Res. Bull.* **1988**, *23*, 447.

(11) *WinPLOTR*; Rodriguez-Carvajal, J. *Physica* **1993**, *B192*, 55.

(12) *X-AREA, IPDS-II Software Package*; STOE & Cie.: Darmstadt, Germany, 2002.

(13) (a) *X-SHAPE, Crystal Shape Optimisation*; STOE & Cie.: Darmstadt, Germany, 2002; (b) *X-RED32, Program for Data Reduction and Absorption Correction*; STOE & Cie.: Darmstadt, Germany, 2002.

(14) Petricek, V.; Dusek, M.; Palatinus, L. *JANA2006, Crystallographic Computing System*; Institute of Physics: Prague, Czech Republic, 2011.

(15) Becker, P.; P. Coppens, P. *Acta Crystallogr.* **1974**, *A30*, 129.

(16) Iliinski, G. A. *Mineral density determination (in Russian)*; Nedra: Leningrad, 1975; p 95.

(17) Suvorov, A.V. *Thermodynamic Chemistry of the Vapor State*; Nauka, Leningrad, 1970; p 208.

(18) Zelenina, V. N.; Titov, V. A.; Chusova, T. P.; Stenin, Yu. G.; Titov, A. A. *J. Chem. Thermodyn.* **2003**, *35*, 160.

(19) Blundell, S. *Magnetism in Condensed Matter*; Oxford University Press: Oxford, U.K., 2009.

(20) Bondi, A. *J. Phys. Chem.* **1964**, *68*, 441.

(21) *TB-LMTO-ASA*; Blöchl, P. E.; Jepsen, O.; Andersen, O. K. *Phys. Rev.* **1994**, *B49*, 16223.

(22) Lee, S.; Foran, B. *J. Am. Chem. Soc.* **1994**, *116*, 154.